Spatiotemporal Evolution of Ground Subsidence and Extensional Basin Bedrock Organization: An Application of Multitemporal Multi-Satellite SAR Interferometry

Carlo Alberto Brunori * and Federica Murgia

Posted Date: 17 February 2023

doi: 10.20944/preprints202302.0286.v1

Keywords: Subsidence; Time Series; PS; InSAR; Valle Umbra Basin; Buried Faults

Article

Spatiotemporal Evolution of Ground Subsidence and Extensional Basin Bedrock Organization: An Application of Multitemporal Multi-Satellite SAR Interferometry

Carlo Alberto Brunori [1,*] and Federica Murgia [2]

[1] Istituto Nazionale di Geofisica e Vulcanologia (Italy); carloalberto.brunori@ingv.it
[2] CREA-Centro Foreste e Legno, Trento; federica.murgia@crea.gov.it
* Correspondence: carloalberto.brunori@ingv.it

Abstract: Since the early 1990s, the European (ESA) and Italian (ASI) space agencies have managed and distributed a huge amount of satellite-recorded SAR data to the research community and private industries. Moreover, the availability of advanced cloud computing services implementing different multi-temporal SAR interferometry techniques allows the generation of deformation time series from massive SAR images. We exploit the information provided by a large PS dataset to determine the temporal trend of ground deformation and the relative deformation rate with millimetric accuracy to analyse the spatial and temporal distribution of land subsidence induced by water pumping from a deep confined aquifer in the Northern Valle Umbra Basin (Central Italy), exploiting 24 years of Permanent Scatterers – Interferometric SAR data archives. The SAR images were acquired between 1992 and 2016 by satellite ERS1/2, ENVISAT and Sentinel 1 ESA missions, and the COSMO-SkyMed ASI mission). We observe ground velocities and deformation geometries between 1992 and 2016, with displacements of more than 70 cm and velocities of up to 55 mm/yr and the results suggest that the shape and position of the surface ground displacement are controlled by the fault activity hidden under the valley deposits.

Keywords: subsidence; time series; PS; InSAR; valle umbra basin; buried faults

1. Introduction

In the last decades, Earth's observation missions have produced a huge volume of data acquired by active and passive sensors operating in several regions of the electromagnetic spectrum, with territorial continuity and very high spatial and temporal resolutions. The International Data Corporation (IDC - www.idc.com) calculates that the total amount of digital data created, replicated, and consumed more than doubles every two years [1]. The storage of this huge amount of data and the analysis techniques needed to extract information is captured in the concept referable to Information Technology as Big Data or, better, Big Earth Data [2,3]. Big Data is the "blanket term" identifying the strategies and technologies needed to store and process large datasets of digitized data [4]. It is a new era of remote observation of the earth's surface that requires new tools, applications, solutions and algorithms that must be invented and developed to fully benefit from the vast amount of information that would otherwise remain under-exploited [3].

The database of products extracted from Earth Observation data and the analysis techniques to retrieve information from themselves are defined as collections of data massive, multi-source, heterogeneous, multi-temporal, multi-scale, high-dimensional, highly complex, non-stationary, and unstructured. Moreover, Big Earth Data can provide a new approach to the development of global changes research techniques [2]. In this framework, the long time-series of Synthetic Aperture Radar (SAR) image catalogues freely available by the national and international Space Agencies (such as the European and Italian Space Agencies, ESA and ASI respectively) can be processed using Multi-temporal Interferometric Synthetic Aperture Radar (MInSAR) techniques, in some cases using cloud computing implementation of processing chains [3, 5, 6] to produce the measure of ground

displacements with high temporal and geometric resolution also at the national scale [7]. The increasing availability of time series produced in the framework of research and applicative projects implementing MInSAR procedures or online services for the generation of land displacement measures allows the monitoring of natural or anthropic phenomena in their evolution.

One of the applications of MInSAR satellite techniques is the monitoring of ground subsidences [8] affecting the anthropized areas such as flat valleys with deformation rates of a few millimeters up to decimetres for a year. The subsidences are mainly related to several processes, often in combination with each other, such as the aquifer-system compaction due to the natural processes or the artificial groundwater extraction for agricultural and industrial purposes and, in certain cases, rapid urbanization can affect unconsolidated alluvial or basin-fill aquifer systems. Indeed, when groundwater migrates from aquifers, the pressure of the water pore decreases, therefore the effective stress in the soils and rocks increases, inducing gradual land subsidence as a consequence of the consolidation of the aquifers [9]. Using MInSAR techniques were observed phenomena of surface ground subsidence correlated to the compaction of sediments such as London [10], Shanghai [11], Mexico City and other cities of Central Mexico [12-14]. In Italy, some areas are interested in ground subsidence such as Roma [15], Bologna town and surroundings [16], the Ravenna coastal plain [17] or the Italian coastlines [18], the whole Po river delta [19], the Venezia lagoon [20], the Arno river basin [21], the Gioia Tauro [22] and Sibari coastal plains [23]. In some cases, the deformations can damage urban infrastructures such as water, gas and electric utilities, buildings and roads [24]. Subsidences have been observed also in areas with dissolution in the subsoil of soluble rocks such as limestone, dolomite, and gypsum or as a consequence of mining [25, 26]. Moreover, several studies on flat valleys try to individuate evidence of fault systems dislocating the bedrock buried under the valley deposits, such as lateral variations of ground deformation velocity [24, 25, 27].

To demonstrate the use of MInSAR time series products this work analyses the slow vertical ground deformations (subsidence) that occurred in a wide territory of Central Italy, the Northern Valle Umbra Basin (NUB), between 1992 and 2016 by exploiting two Permanent Scatterers (PS) datasets derived from 24 years (1992-2016) of SAR data (Figure 1). Four satellite missions acquired the SAR data employed for the NUB subsidence analysis: ERS 1-2 (ERS), ENVISAT (ENV), COSMO-SkyMed (CSK) and Sentinel 1 (SNT). MInSAR soil displacement time series was produced within two projects: 1) the Piano Straordinario di Telerilevamento Ambientale (PST-A; “Extraordinary Plan for Environmental Remote Sensing”), funded by the former Italian Ministry of Environment, Land and Sea (MATTM http://www.pcn.minambiente.it/) and 2) the ESA project MEMPHIS (Multi-scale and Multi-Hazard Mapping space-based Solution project and processed by ALTAMIRA-TRE (Figure 1 a and b, Tables 1 a and b)

Preprints (www.preprints.org) | NOT PEER-REVIEWED | Posted: 17 February 2023 doi:10.20944/preprints202302.0286.v1

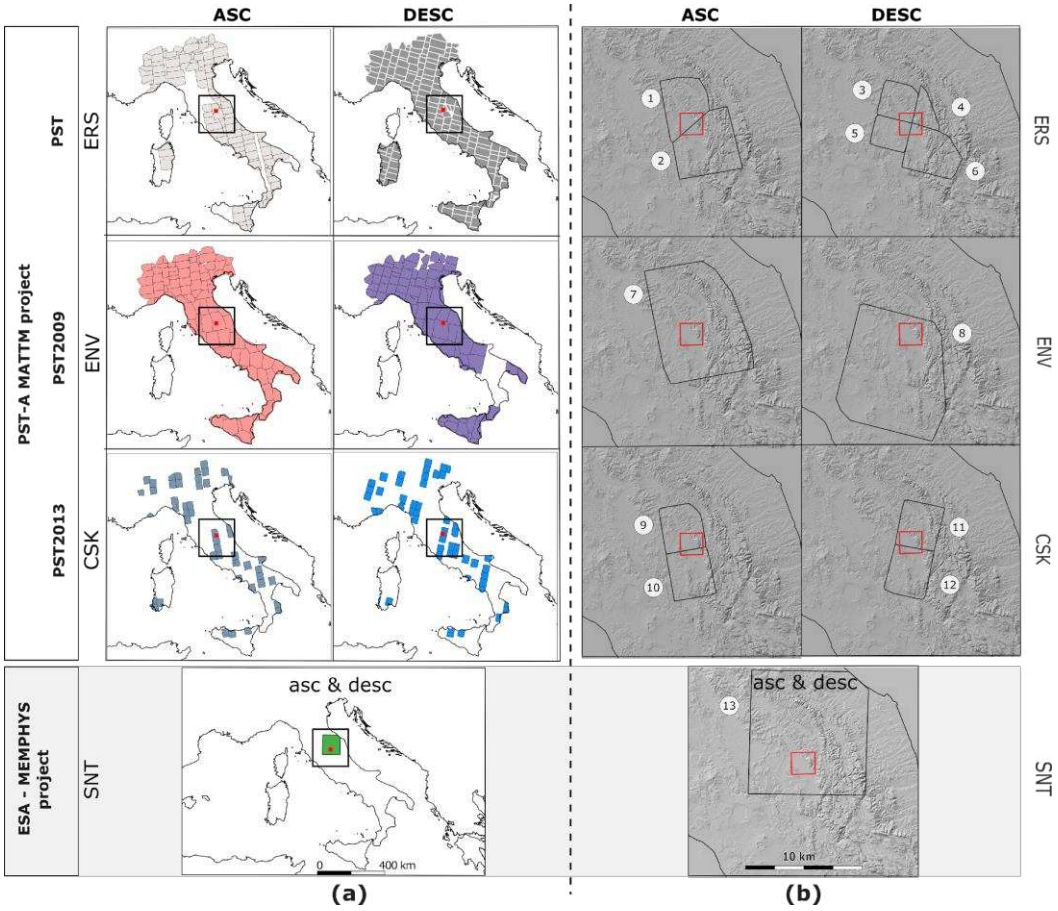

Figure 1. (a) The PS data in the Italian peninsula provided by the PST-A project (in the first three rows the data from 1992-2014 ERS, ENV and CSK, missions) were organized in clusters of the ascending (ASC) and descending (DESC) orbits. In the last row, the Italian area covered by PS is derived from the SNT mission in both ascending and descending satellite orbit data, processed by the ESA-MEMPHIS project. See Tables 1a and 1b for the statistics. The black box locates in Figure 1b area. (b) The red box locates the NUB study area and the numbers in the white circles identify the clusters' names (Table 3) used in this work. In the background, the central Italy orography and black boxes are the clusters of PS used in this work.

Table 1. (*Upper panel*) The tables summarize the statistics of a) *surfaces* for all clusters of the three satellite missions of the MATTM database (ERS; ENV, CSK). *(Lower panel) number of* PS *for cluster* in the MATTM database (ERS; ENV, CSK) and in the MEMPHYS database (SNT).

Preprints (www.preprints.org) | NOT PEER-REVIEWED | Posted: 17 February 2023 doi:10.20944/preprints202302.0286.v1

		ERS		ENV		CSK	
		ASC	*DESC*	*ASC*	*DESC*	*ASC*	*DESC*
Clusters #		117	201	110	95	56	56
kmq	Sum	238.250	321.270	316.163	272.516	76.214,6	76.843,4
	Max	4.406,61	4.576,96	8.288,59	9.871,27	1.954,86	2.015,38
	Min	13,68	6.241	2.725	3.532	5,319	14,097
	Mean	2.036,33	1.598,36	2.874,21	2.868,59	1.360,97	1.372,2
	Median	1.992,97	1.613,93	2.530,64	2.681,33	1.538,24	1.562,31

		ERS		ENV		CSK		SNT	
		ASC	*DESC*	*ASC*	*DESC*	*ASC*	*DESC*	*ASC*	*DESC*
Numb. of PS		4.378.310	9.438.651	15.359.988	12.895.230	65.019.955	63.735.666	611.986	721.982
Numb. of Clusters		117	201	110	95	56	56	1	1
PS/kmq (avg.)		2.150,1	5.905,2	5.344,1	4.495,3	47.774,7	46.447,8	51,58	60,85
kmq	Max	218.468	264.282	747.622	756.312	4.601.190	4.242.770		
	Min	881	518	205	258	20.969	4.940		
	Mean	37.744	47.193	139.635	135.739	1.154.140	1.051.230		
	Median	27.902	34.248	72.690	70.995	872.943	893.517		

In the following, after an overview of the geological settings of the area and a presentation and quality check of the exploited PS dataset, ground deformation using the displacement and velocity maps derived from PS datasets. Therefore, it is described and discusses the relation between 1) ground subsidence and the variation of the piezometric level in the wells extracting water from a deep-confined aquifer; 2) how the location of surface soil displacement and valley morphology may be driven by the activity of faults that dissect the bedrock under the valley deposits.

2. Case study

Ground subsidence occurring in the Northern sector of the NUB [29] is measured using PS data generated by exploiting MInSAR techniques. The NUB (also called "Spoletana" Valley) is an NNW-SSE 20 km long and 10 km wide and flat valley located west of the "inner ridge" of the Northern-Central Italian Apennines [30 - 32] (Fig 2). The local highest elevation is 1.290 meters of Mt. Subasio, and the valley has elevations between 170 m.a.s.l. near the Northern confluence with the Tevere Valley and 240 m.a.s.l. on the Southern side, in Foligno town (on the Topino river conoid Figure 2). Principal cities of the area are Perugia and Foligno. Perugia town, with about 163.000 inhabitants, is the capital city of both the Umbria Region and of the homonymous Province, is located on the right side of the Tevere river Valley at the junction with the NUB in their Northernmost limit. Foligno (55.300 inhabitants), is located in the Southernmost limit of the studied area. The valley is anthropised with intense agricultural activities and several industrial settlements. Principal towns and villages of the NUB are, from North to South: Santa Maria Degli Angeli, Assisi, Tordandrea, Cannara, Bastia, Foligno, Spello, Bevagna and Foligno (Perugia Province, Umbria Region – Figure 2).

Preprints (www.preprints.org) | NOT PEER-REVIEWED | Posted: 17 February 2023 doi:10.20944/preprints202302.0286.v1

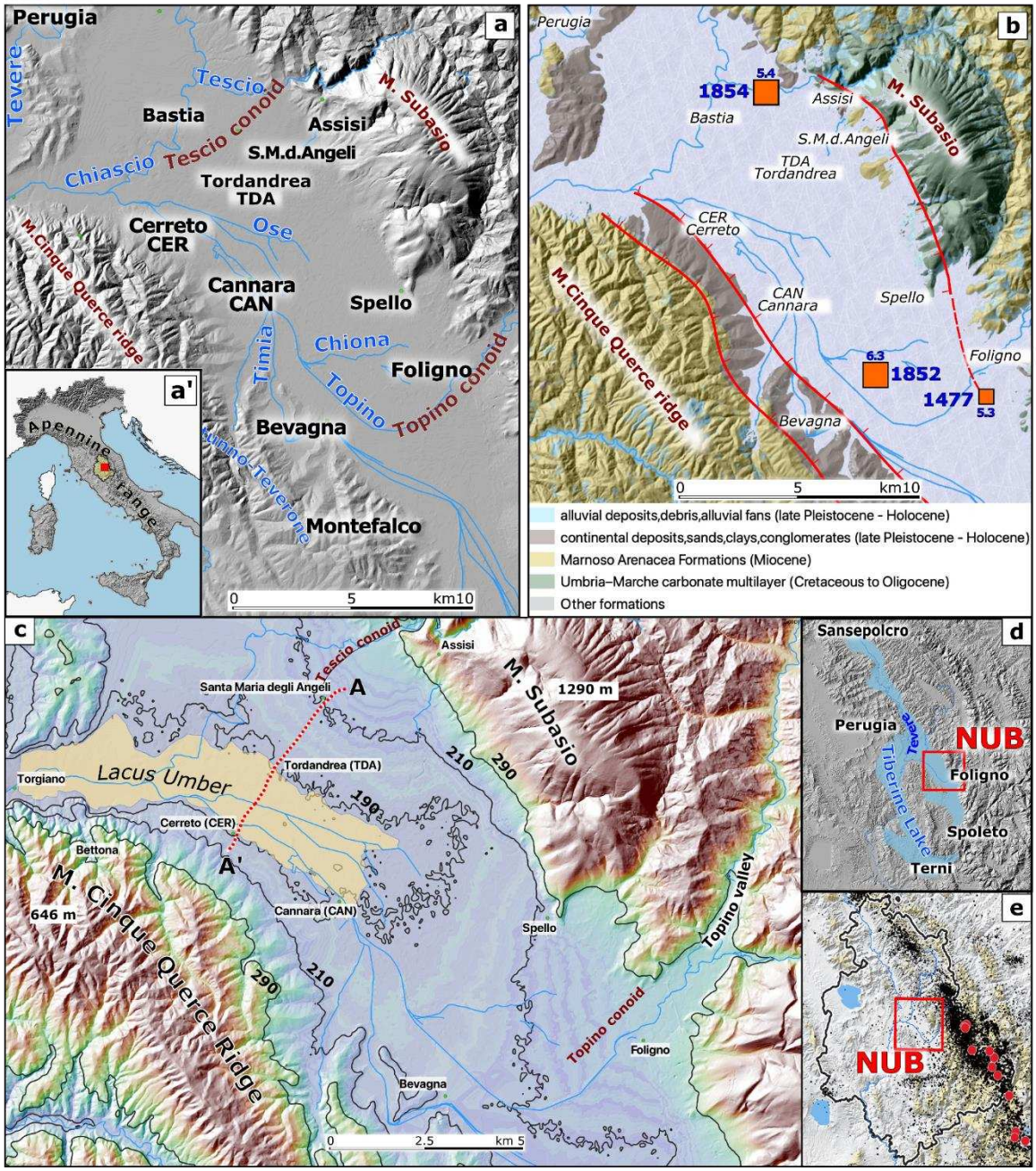

Figure 2. a) Principal towns, mountains and rivers of the NUB. a') The Italian peninsula with the Umbria region (light yellow polygon), the red dot locates the NUB. b) Geology map of the NUB area: red lines are the normal fault traces (the vector layers were provided by Regione Umbria WEBGIS service), *and* the shaded relief in the background is derived from *TINIT* DTM *[33]*; toponyms and rivers vectors were provided from Italian ISTAT portal (https://www.istat.it). The orange box locates the epicenters of three main historical earthquakes (Rovida et al., 2021*)* with the equivalent Magnitude and year of occurrence. c) The NUB orography: the black lines are the isolines showing the valley asymmetry and the shape of the alluvial conoids; the light yellow area locates in the sector with the valley's lower elevations, this area was occupied by a large lake and marshy area called "Lacus Umber" *[34]*. The A-A' red dots locate the topographic and PS velocity profiles of Fig 9. d) The Tevere valley with Northern and the Southern NUB formed the Plio-Pleistocenic Tiberine Lake (light blue area). e) The Umbria Region border and the cloud of small black dots (2.5< M < 5) and red circles (M>=5.0) are the 1990-2022 seismicity of this sector of the Apennine chain.

The NUB is the eastern segment of the Tevere Basin, the former "Tiberine lake", a Plio-Pleistocene lacustrine basin (Fig 2d) whose sediments filling the valley were deposited in an

 doi:10.20944/preprints202302.0286.v1

environment characterized by braided rivers and shallow lakes [35 - 39]. The Tevere basin, with an area of about 1800 km2, is the largest of the intermountain basins in the Umbria region (Figure 1). Crossing entirely the region from the northern basin of Sansepolcro southwards, it divides into two segments near Perugia, the western branch extends southwards, in part along the Tevere river, while the eastern one is the NUB [37]. The NUB (Figure 1), is a 180 km2 -wide intermontane depression formed in response to the extensional tectonics dissecting the pre-existing fold-and-thrust belt system during the Quaternary period. The Plio-Pleistocene continental sequence infilling the NUB consists of a complex succession of laterally discontinuous deposits, mainly composed of lignitiferous clays, sands, sandy clays and conglomerates. The alluvial sequence is more than 150-200 m thick [40] with lateral variations due to the presence of fluvial conoids (mainly the Topino and Chiascio alluvial fans, Figure 1) and the structural organization of the underlying bedrock. The Jurassic to Eocene bedrock overlayed by the Quaternary to recent formations sequence outcropping in the area, from the youngest to the oldest, is composed of: the recent and old fluvial and alluvial deposits with fine sand and silt levels, lenses of coarse gravel and sand and, locally eroded by fluvial terraces [41]; the continental sequence of depositional environments characterized by braided rivers and shallow lakes (Bevagna Unit in Figure 2b) [35 - 39, 42] outcropping extensively in the South-Eastern limits of the NUB [37] (https://dati.regione.umbria.it/dataset/carta-geologica-dell-umbria) [39]; the Marnoso Arenacea Formation (early to middle Miocene) [43] and the Cretaceous to Oligocene Umbria–Marche carbonate multilayer of pelagic origin with, at the bottom, the limestones formed in shallow-water platforms in the lower Liassic (Calcare Massiccio Formation) [44, 45]**.** The Upper Miocene Marnoso Arenacea formation (Figure 2b) outcrops in the M. Cinque Querce Ridge (SW of NUB), at the confluence of the Chiascio and Tevere and on the Northern side of the study area near the Torgiano village. Moreover, the Marnoso-Arenacea formation is present along Mt. Subasio slopes and constitutes the bed of the valley's alluvial and lacustrine deposits.

The Mt. Subasio ridge is dominated by the Umbria-Marche carbonate multilayer (Northern Appenninic Meso-Cenozoic limestone successions). The area was affected by extensional tectonics since the upper Pliocene – early Pleistocene [31, 46] and the 0.5 mm/year of regional uplift competes with the regional subsidence due to the activity of the local normal faults producing subsiding basins incised by modern rivers [47]. The principal NUB watercourses are the Chiascio (length 82 km, 19 m^3/s averaged discharge, drainage area 1843 km^2), Topino (length 76.6, 10.5 m^3/s averaged discharge, drainage area 1031 km^2) and Clitunno (length 59.3, 3.6 m^3/s averaged discharge, drainage area 701.4 km^2) and the minor ones Tescio, Ose, Chiona and the Marroggia-Teverone-Timia streams (Figure 2a).

The Topino river is flowing in the NUB from the Topino Valley (from NE toward SW), then rotates 90° toward NW and, after receiving the waters of Marroggia-Teverone-Timia and Chiona streams and their tributaries, flows northward inside straight and narrow artificial banks and in part parallel to the tributaries, then flow into the Chiascio river near their confluence into the Tevere river. Both the Chiascio and Topino rivers flow initially from North to South and, after crossing the valley, intercept the water of Clitunno and Marroggia flowing from SE and after rotating toward NW, flow on the south-eastern side of the valley. In the NUB are present conoids only on the Western side of the valley because of the greater size of the catchment areas of rivers coming from the Apennines and by the presence of a segmented system of both ENE-dipping with prevalent activity, and the WSW-dipping active normal faults along the SE and NW sides of the NUB, SE-NW striking, dissecting the pre-existing (Late Miocene) compressional structures of the Umbria-Marche Apennines (Figure2c) [46, 48, 49]. This fault system is visible along the M.Subasio and Mt. Cinque Querce ridge slopes, forms the NUB graben, and is probably also hidden under the Quaternary sediments filling the NUB [50]. The activity of these structures is also suggested by the distribution of both instrumental and historical seismicity (Fig 1b-e) [51]. Among the long sequence of earthquakes that struck the valley (CPTI15 - https://emidius.mi.ingv.it/CPTI15-DBMI15/), this area experienced in the 19th century two major earthquakes with the epicenters here localized: the 13 January 1832 ME=6.3; I0=X, and the 12 February 1854 ME=5.6; I0=VII (Figure 2b). In recent times the earthquake sequences affecting the Apennine sector East of the NUB and the Monte Cinque Querce Ridge (Figure 1e), hit the valley and the urbanized areas, such as the 26 September 1997 (Mw 6.0), often causing considerable damage to civil and industrial structures as well as to technological networks mainly due to local amplification effects [50].

The NUB is characterized by diffuse and intense agricultural activities and the fields of wells extracting water from confined aquifers are localized at the confluence area of all the NUB rivers, the principal depocenter

Preprints (www.preprints.org) | NOT PEER-REVIEWED | Posted: 17 February 2023 doi:10.20944/preprints202302.0286.v1

of the NUB, the NW flat sector of the valley (Tordandrea -TDA area; Fig 2d), this is a flat area that, up the XVII century, may have hosted the basin known in the literature as Lacus Persius (Persius lake) [52] or the more extended Lacus Umber (Figure 2c, Umber lake) [34]. This area experienced the last up to 30 years of the subsidence phenomena described in the following paragraphs.

3. Materials and Methods

By using well-established multi-temporal interferometric techniques, the whole ESA dataset of SAR images covering the Italian territory acquired by ERS, ENV and CSK satellites relative to 1992-2000, 2002-2010 and 2011-2016 time intervals respectively, were processed in the framework of the PST-A project (http://www.pcn.minambiente.it/.). The PS products of the PST-A project are freely distributed by the Ministry of Environment and Energy Security as shapefiles (points) containing time series data of ground displacement values for both ascending and descending satellite Line of Sight (LOS) and deformation rate (Figure 1a). The ERS images (1992-2000) were undertaken by Tele Rilevamento Europa Srl (TRE) using the PSInSAR technique [53], the ENV data (2002-2010) were processed by eGEOS with the PSPDIFSAR approach [52] (Costantini et al. 2009). The CSK image data (2011-2014) were processed with the PSP-IFSAR analysis algorithm [54], but the spatial coverage of the CSK dataset covers only a few areas (Figure 1a). The 2014-2016 SNT PS database covering a wide sector of the central Italy peninsula (Fig 1a), was provided by the ESA MEPHYS project and processed by ALTAMIRA-TRE using the SqueeSAR technique [53] and by exploiting the PSI Post-Proc tool, available on the GEP processing services (Geohazards Tep web portal. https://geohazards-tep.eu). The GEP processing services made it possible to calculate the averaged accelerations associated with each PS in the scenes (Tables 1 and 2) and to decompose the LOS deformation into the Up-Down (UD) and East-West (EW) components.

Table 2. The 1993-2016 PS dataset covering the study area, derives from SAR data acquired by four satellites carrying sensors operating in the C (ERS, ENV and SNT) and X bands (CSK). The first set of images (1993-2014), was acquired by the ESA ERS satellite (1992-2000), ESA ENV (2003-2010) and by the Agenzia Spaziale Italiana (ASI) CSK satellite constellation (2011-2014). The last set of images was acquired by ESA SNT (2014-2016). The dates are expressed in the dd/mm/yyyy format.

	ERS 1-2	ENV	CSK	SNT1
Band (wavelen. cm)	C-band (5.6)	C-band (5.6)	X-Band (3.1)	C-band (5.6)
Operation mode	SAR/IM (1)	SAR/IM (1)	HIMAGE (Stripmap)	StripMap (HIMAGE)
Revisit cycle days	35	35	16	12
Look angle	23°	23°	25°-57°	329°
Swath km	100	100	40	240
ASC n. images	35	51	40	48
ASC first image	02/04/1995	02/12/2002	09/05/2011	25/10/2014
ASC last image	23/10/2000	24/05/2010	30/03/2014	21/08/2016
DESC n. images	56	37	30	42
DESC first image	21/04/1992	10/10/2003	29/07/2011	24/10/2014
DESC last image	29/12/2000	25/06/2010	16/04/2014	01/09/2016

Table 3. The PS dataset: the satellite missions, orbits, project identification code and project identification file name and list of PS clusters used for the analysis in this work of the NUB area (see Figure 1b).

Preprints (www.preprints.org) | NOT PEER-REVIEWED | Posted: 17 February 2023 doi:10.20944/preprints202302.0286.v1

	orbit	Project ID	Cluster ID	# Fig 1b
ERS 1-2	**ASC**	PST	ERS_T401_F858_CL003_SPELLO	1
			ERS_T401_F858_CL004_SPOLETO	**2**
	DESC	PST	ERS_T351_F2745_CL002_PERUGIA	3
			ERS_T79_F2748_CL001_GUALDO	4
			ERS_T79_F2748_CL003_SPOLETO	5
			ERS_T351_F2745_CL001_MARSCIANO	**6**
ENV	**ASC**	PST2009	ENVISAT_T401_F858_CL001_ASSISI	**7**
	DESC	PST2009	ENVISAT_T351_F2745_CL001_TERNI	**8**
CSK	**ASC**	PST2013	CSK_F_44_PERUGIA_A_CL001	9
			CSK_F_43_SPOLETO_A_CL001	**10**
	DESC	PST2013	CSK_F_46_SPOLETO_D_CL001	11
			CSK_F_45_GUALDOTADINO_D_CL001	**12**
SNT	**ASC**	SqueeSAR	S1_T117_A_33	**13**
	DESC	SqueeSAR	S1_T95_D_32	**13**

Preprints (www.preprints.org) | NOT PEER-REVIEWED | Posted: 17 February 2023 doi:10.20944/preprints202302.0286.v1

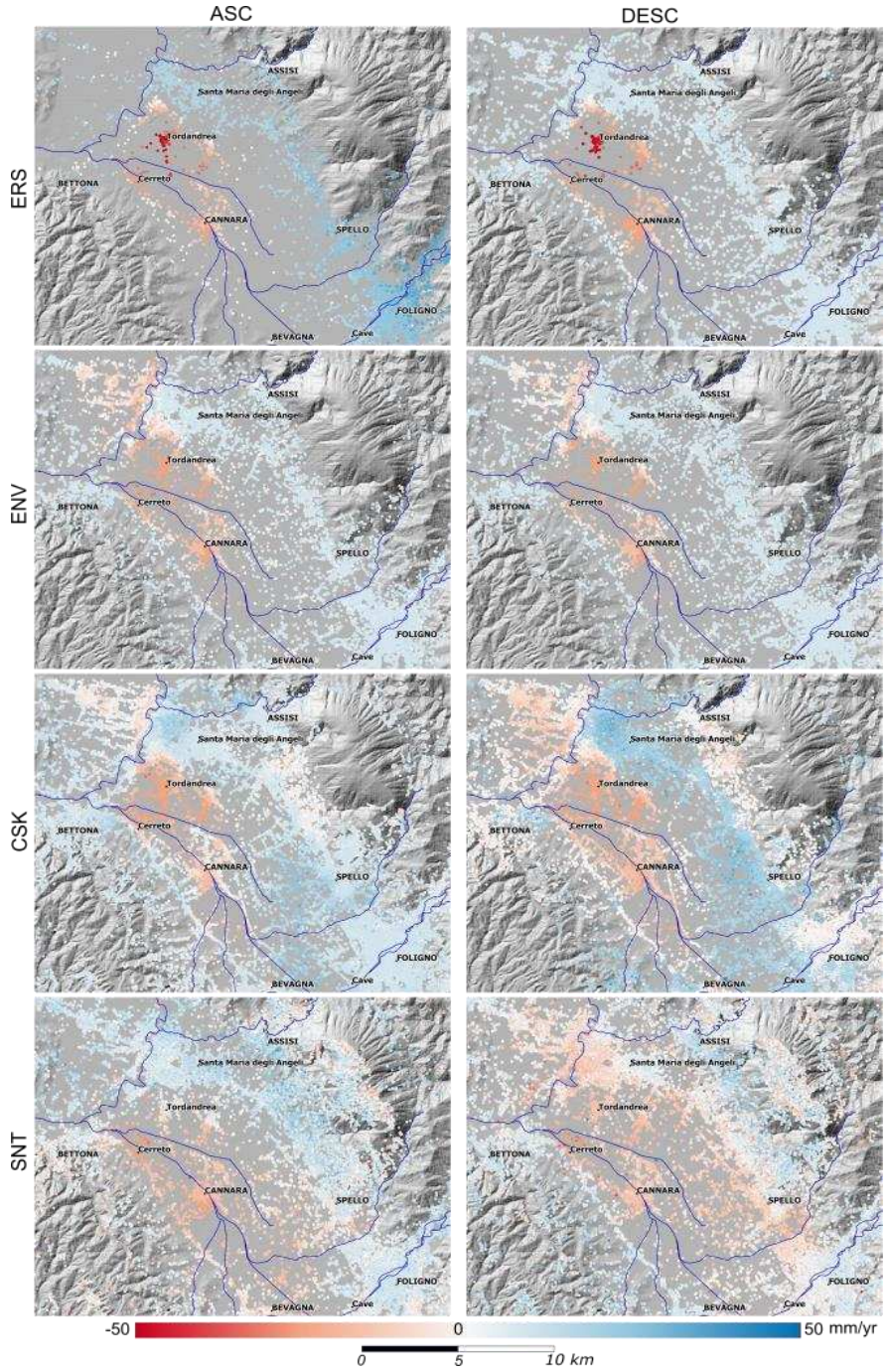

Figure 3. Velocity maps in the LOS direction for each of the PS datasets *were* retrieved from the independent processing of the ascending (left panels) and descending (right panels) SAR image stacks respectively.

The analysis is focused on the flat sector of the NUB where the velocity maps show negative ground velocities (i.e. the ground surface moves away from the satellite) during 1992-2016 in the northern side of the valley (Figure 3). Notwithstanding the time gaps between the four satellite acquisitions (Table 1), for the whole observation period a linear trend of the ground vertical deformation is assumed [6, 13]. Furthermore, to compare different satellite measurements, the CSK and SNT LOS time series were re-projected on the ERS and ENV LOS [13]. Then, each ERS, ENV, CSK and SNT LOS mean velocity map, both on ascending and descending tracks, have been post-processed and compared to assess quantitatively the reliability of the datasets. The comparison between the ascending and descending tracks within the region of interest shows good correlations for the ERS, ENV and CSK (R2 = 0.95, 0.93 and 0.84 respectively, Figure 4). These values indicate that the subsidence patterns obtained from the three datasets are dominated by vertical motion. On the other hand, the SNT datasets show a complex distribution of values probably due to the presence of the East-West slow

Preprints (www.preprints.org) | NOT PEER-REVIEWED | Posted: 17 February 2023 doi:10.20944/preprints202302.0286.v1

component of the ground movement. However, for values characterized by a velocity greater than -10 mm/yr a continuity in the vertical displacement in both ascending and descending datasets is visible.

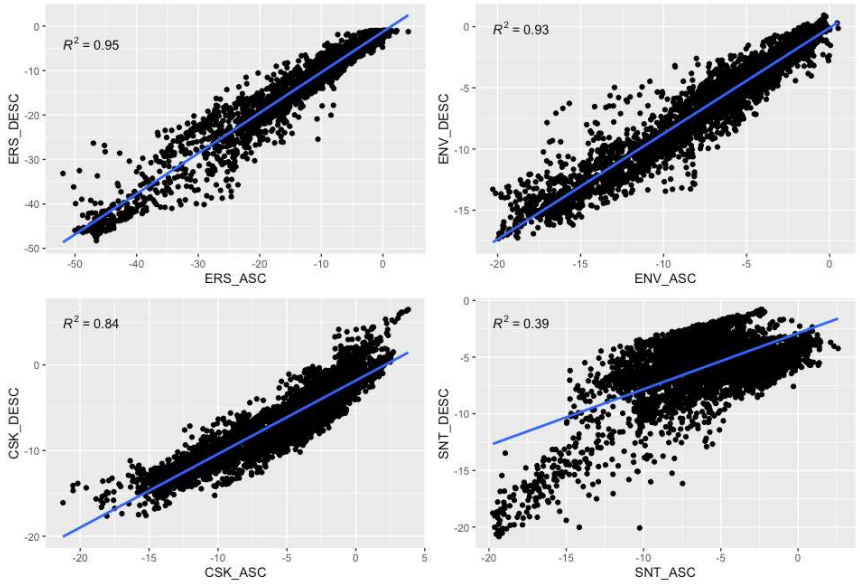

Figure 4. For each satellite, the ground velocities in the subsiding area are compared by plotting the common ascending and descending pixel values in the horizontal and vertical axis respectively, the values are expressed in mm/yr. Black points are the velocities of the whole subsiding study area. The blue line is the linear interpolation, and the R2 values are reported. The ground velocities for ERS, ENV and CSK are comparable for both ascending and descending orbits with R2 close to 1, while the SNT velocities show values more dispersed (with a much lower R2) than in the previous periods.

We focus the attention only on vertical displacements, other (East-West) displacements and the minor signals are not taken into account in this work. Three selected sites of the NUB are selected to analyze the ground displacement: Tordandrea (TDA) and Cerreto (CER) areas with the highest deformation rates, and Cannara (CAN) with intermediate behaviour in terms of ground velocities (Figure 2a, 3). The ERS, ENV and CSK ascending and descending datasets were combined to retrieve the vertical (Up) and East-West (East) velocity field (Fig 5) [13, 56]; by using 100 m square elements to resample to a regular grid the PS point datasets from both tracks. The Up and East values were achieved by applying Eq. 1 and assuming null or negligible North–South velocity because of the quasi-polar orbit of the satellite and the right lateral observation geometry [56, 57].

$$Up = \frac{V_d sin\theta_a - V_a sin\theta_a}{sin(\theta_a + \theta_d)} \qquad East = \frac{V_d cos\theta_a - V_a cos\theta_d}{sin(\theta_a + \theta_d)} \tag{1}$$

The observed vertical velocities (Figure 5, Tab 4) show that for the ERS dataset (1992-2000) the highest vertical velocity is ~51 mm/yr with a total ground displacement of ~-445 mm in the TDA area. For the ENV data (2002-2010) the maximum velocity value is moving SW toward the CER area decreasing to -20,1 mm/yr, and with a displacement of -152 mm. In the same area in the 2011-2014 (CSK) and 2014-2016 (SNT) periods, the ground velocities are, respectively, -15 mm/year (with a total displacement of ~ -116 mm), and -16 mm/year (displacement of ~ -47 mm). In the CAN area, the vertical velocity decreased between 1992 and 2010 (ERS, ENV and CSK acquisitions), stabilising during the period of the SNT acquisition (Table 4). The cumulate displacement i.e. in the TDA area is 620,3 mm, but the value doesn't take into account the satellite acquisition gaps

Table 4. The ground velocities and vertical ground displacements in three selected areas (CAN, CER and TDA), measured by four satellites (ERS, ENV, CSK and SNT).

	ERS 1992-2000	**ENV 2002-2010**	**CSK 2011-2014**	**SNT 2014-2016**	*Total displacement*
Years	*8,74*	*7,56*	*2,94*	*1,86*	

Preprints (www.preprints.org) | NOT PEER-REVIEWED | Posted: 17 February 2023 doi:10.20944/preprints202302.0286.v1

	mm yr	mm	**mm yr**	mm	**mm yr**	mm	**mm yr**	mm	*mm*
TDA	**-50,9**	-444,9	**-15,3**	-115,7	**-16,2**	-47,6	**-6,5**	-12,1	*-620,3*
CER	**-33,2**	-290,2	**-20,1**	-152,0	**-19,7**	-57,9	**-23,0**	-42,8	*-542,8*
CAN	**-15,9**	-139,0	**-13,4**	-101,3	**-10,7**	-31,5	**-11,3**	-21,0	*-292,7*

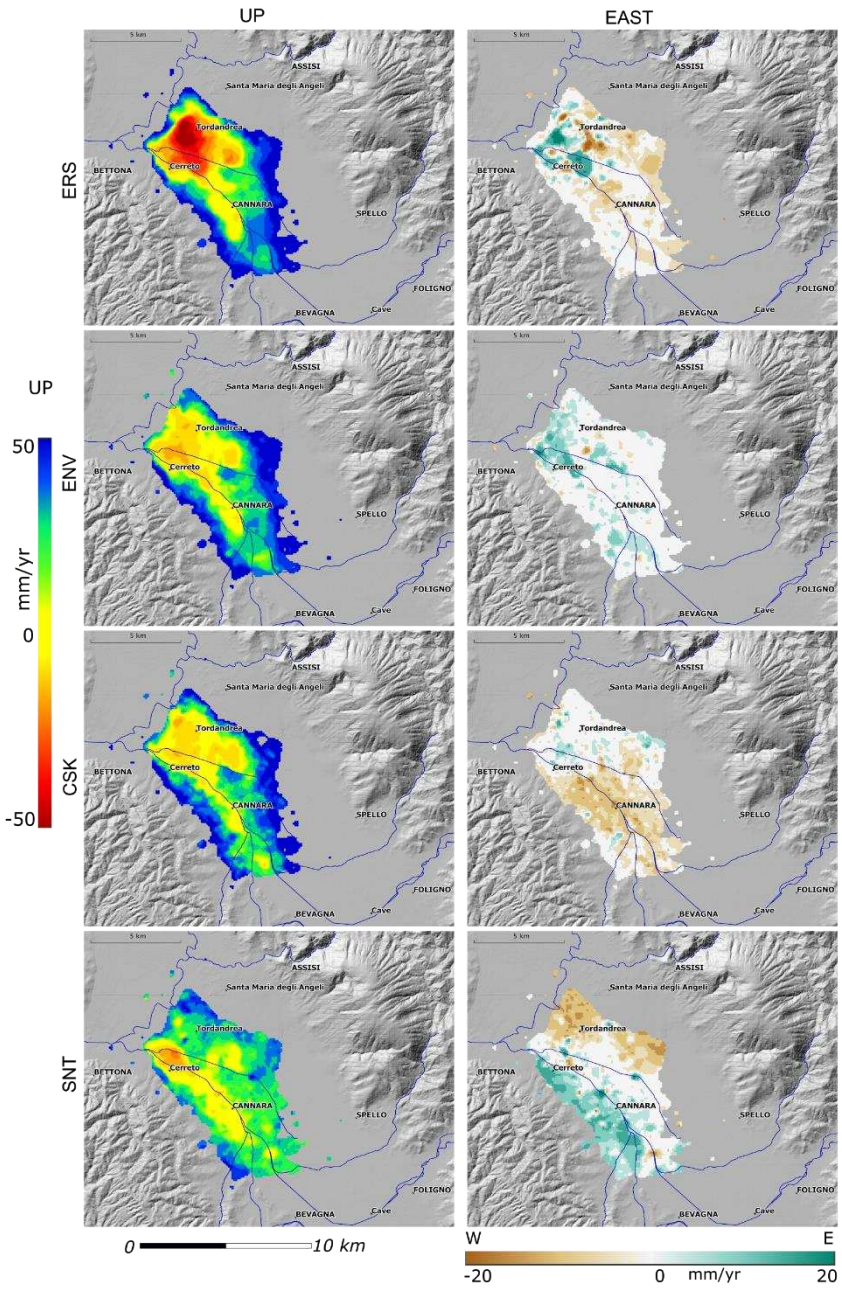

Figure 5. Velocity maps for Up (vertical displacements) and East-West (horizontal displacements) velocity components (mm/yr) in the NUB area during time intervals: a) 1992 - 2000 [ERS, 1st row]; b) 2002 - 2010 [ENV, 2nd row]; c) 2001 - 2014 [CSK, 3rd row] and 2014-2016 [SNT, 4th row].

4. Discussion

The subsidence observed in the NUB is analyzed by exploiting available datasets of MInSAR products. Moreover, the observed deformation trend during the 1996-2002 time interval is compared with the piezometric levels time series measured in some of the wells of the same area (in particular

 doi:10.20944/preprints202302.0286.v1

P9, P16 and P26 wells, Figure 6d). Although the SAR acquisitions of the four exploited satellites (ERS, ENV, CSK, SNT. Table 2) do not have a time cover continuity to directly extrapolate measures of ground displacement, the time gaps were filled by applying a linear fit to the different displacement intervals to obtain a continuous measure of the deformation (Fig 6a, b, c). The subsidence calculated using available PS values in the TDA area is up to -70 cm (Figure 6d). After the integration of the four datasets, the deformation series were compared with local groundwater levels time series (Fig .6a, b, c, the well's water level measures are provided by Arpa Umbria, https://apps.arpa.umbria.it/acqua/contenuto/Livelli-Di-Falda). Since 1990 the artesian aquifer localized in the northern NUB, known in the bibliography as the "Cannara aquifer" (ARPA 2007 - https://www.arpa.umbria.it/resources/docs/ACQUIFERI_valle_umbra.pdf) [59], has undergone intense pumping for drinking water uses. Historical data show that at the beginning of the 1970s, the piezometric level in this area was about 10 meters from the ground level, (around 198 m. s.l.m). Later on, at the end of the 1980s, the groundwater level was around 188-190 m a.s.l.

The entry into operation of the field of wells, with increasing withdrawals up to 250 l/s, led to the significant depression of the aquifer. In 1990-2002 there was a decrease in the height of water in the wells of the observed subsiding TDA area, while the data available for the following period (2005-2020) show a positive trend in the level of water, in particular, in the well P26 (Figure 6a). In the CAN area (Figure 6c), as in the TDA area, the observed 1992-2016 subsidence is accompanied by a positive trend of the P16 well water levels. On the contrary, in the subsiding CER area, the negative trend of the 2004-2019 water levels in the P9 well and the continuous lowering of the ground surface are well correlated (Figure 6b). In summary, the piezomter of the P26 shows that the water level has increased by 7 m on average during 2006-2016. The well's water fluctuations are also visible due to seasonal intermittent water withdrawals for agricultural purposes in combination with the water inputs due to rainfalls; these oscillations are also visible in the deformation time series with reduced dynamics. The deceleration of the ground velocity for the P26 surroundings can be interpreted as a consequence of the deep aquifer compaction [29, 59] (Guzzetti et al. 2009; Beretta et al. 2018) due to excessive water withdrawal. In the P16 the average water level shows a positive trend between 2006 and 2016 and the ground subsidence trend is constant. A different behaviour can be observed in P9 where both the water level and the soil's lowering trend have a negative sign.

Preprints (www.preprints.org) | NOT PEER-REVIEWED | Posted: 17 February 2023 doi:10.20944/preprints202302.0286.v1

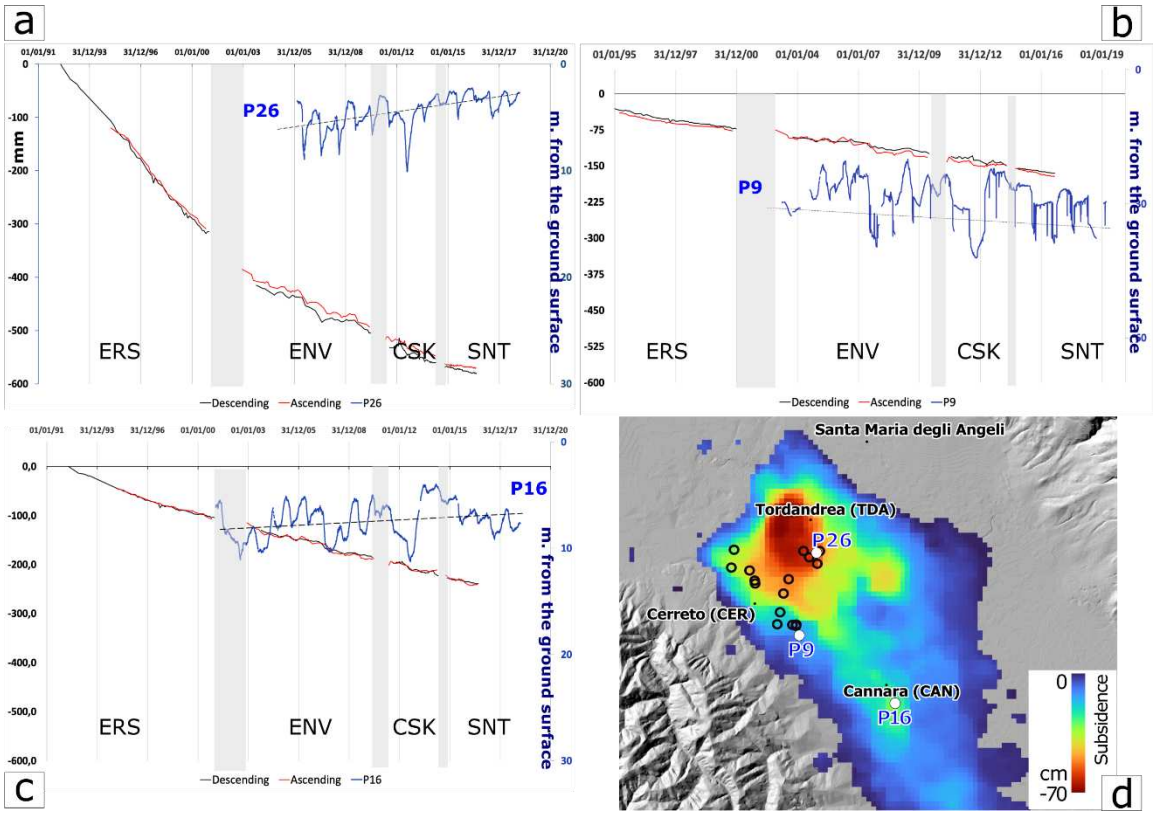

Figure 6. *(*a, b, c*)* Ground displacements measured by satellites in the descending (black lines) and ascending (red lines) LOS expressed in mm in three selected zones in correspondence of P9, 16 and 26 wells. The PS time series were compared to the water levels (blue lines are the water level in the wells from the surface expressed in meters)*(*a*)* Tordandrea (TDA) and P26 water levels; *(*b*)* Cerreto (CER) and P9 water levels; *(*c*)* Cannara (CAN) and P16 water levels. *(*d*)* Total subsidence map measured by ERS, ENV, CSK and SNT satellites between 1992 and 2016, black circles between TDA and CER are wells of the Cannara wells fields, and the white circles are the P9, 16 and 26 wells.

In February 2019 using the Differential Global Positioning System (DGPS) technique, a topographic campaign produced a detailed elevation profile crossing the TDA area (Fig 8a) from the stable area on the eastern side of the valley (S. Maria Degli Angeli village) through TDA and toward CER area. Along the profile maximum elevation difference is -33 m between stable areas and the subsiding zone (TDA) with two steps correlated to the changes of ERS, ENV, CSK and SNT ground velocities measured along the same elevation profile trace (Figure 7a). The velocity and topography steps can be correlated to the presence of hidden faults dislocating the bedrock (Figure 7b).

Preprints (www.preprints.org) | NOT PEER-REVIEWED | Posted: 17 February 2023 doi:10.20944/preprints202302.0286.v1

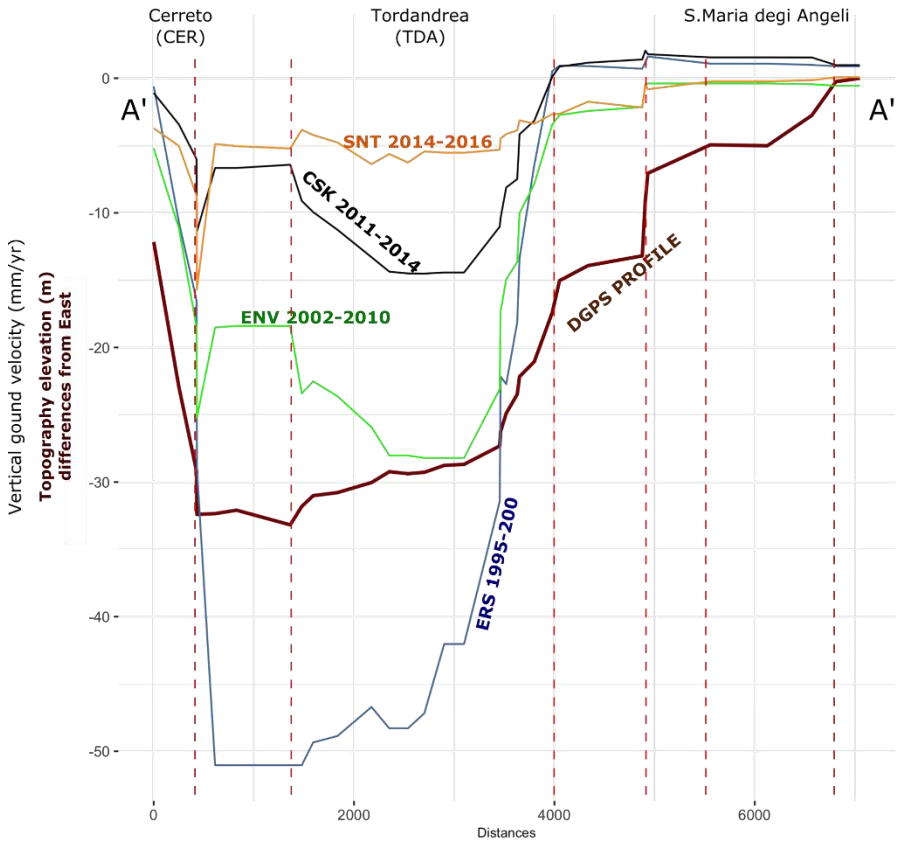

Figure 7. *(Upper panel)* Topographic and velocity profile: the brown line is the elevation profile of the valley along A-A' (Figure 3c), and the blue, green, black and orange lines are the ERS, ENV, CSK and STN satellite's ground vertical velocities profiles respectively along the same profile. The Y axe values are vertical velocities (mm/yr) and elevation differences in meters. The red dashed lines identify the orographic steps along the profile that are correlated to the changes in ERS, ENV, CSK and SNT ground velocities measured along the same elevation profile trace (horizontal vs. vertical scale is 1:100). (*Lower panel*) Schematic and out-of-scale geological profile along the A-A' trace (mod. [48]): (MA) Marnoso Arenacea Formation; (UMC) North Appeninic Carbonate multilayer; (BU) Bevagna Unit; (QD) Quaternary deposits.

2. Conclusions

During the last decades the availability of very large datasets of SAR satellite acquisitions and new technologies based on advanced cloud computing implementing the multi-temporal differential interferometry (MDInSAR) technique, allows the observation of the earth deformation phenomena with unprecedented time and areal extensions in the framework of the Big Earth Data.

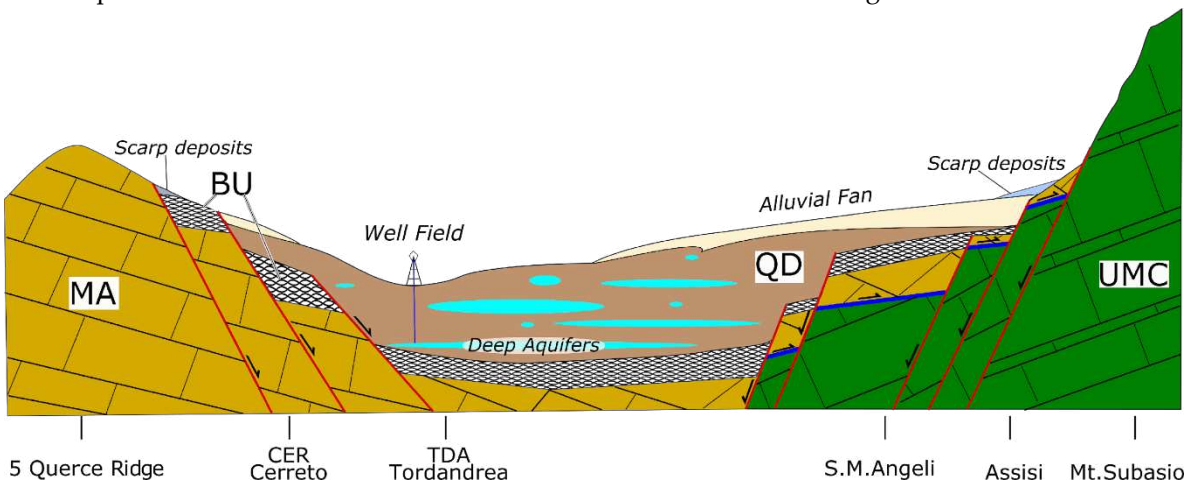

To take advantage of the opportunities offered by the availability of long-time series of satellite data and online advanced data processing technologies, here are used the SAR image acquired by ERS 1-2, ENVISAT, Sentinel-1 ESA satellite missions and the Cosmo-SkyMed ASI mission, and elaborated within the ESA-MENPHYS (Sentinel 1) and the Italian projects MATTM-PST-A (ERS, Envisage and Cosmo-SkyMed) to produce time-series of ground displacements PS datasets. The ground subsidence that occurred in Central Italy is analyzed in temporal and geometric terms by exploiting the 1992-2016 datasets of ESA-MENPHYS and MATTM-PST-A MInSAR PS products. The PS time series, cover the entire observation period with time intervals between satellite acquisitions. The ground displacements and velocities in both ascending and descending satellite geometries acquisitions were analyzed and post-processed to produce maps of a total deformation trend in the LOS and the vertical and horizontal (East-West) velocities components. During the observation period, the subsidence has been predominantly vertical with a progressive decrease in the rate of displacement, progressively moving the depocenter towards the southwest. Moreover, the time series of the deformation relative to the most deformed area (TDA - Tordandrea) has been compared with the piezometric level data provided by ARPA Umbria archives. Although with different dynamics, the ground deformation and groundwater levels show periodical oscillation, mostly visible in the piezometers data, due to the alternation of overexploitation of groundwater reserves and periods of recharge. The ground subsidence correlated with the intense artificial water withdrawal from the deep local aquifer and the shape of the deformation gives information about the shapes of bedrock geometries hidden under the valley deposits. [50] confirmed that under valley sediments is present the NW-SE trending fault system SE dipping faults dislocating northern-eastern lithologies of the Mt. Subasio and in the NW dipping of the Cinque Querce ridge (Figure 1). The NE dipping fault system is considered the source of the historical earthquakes hitting the valley in 1832 and 1854 (Figure 1b. DISS working group, 2021). The over-pumping from the confined groundwater of Cannara aquifer causes the irreversible collapse of the aquifer, highlighted by the ground surface subsidence that is up to 70 cm in the TDA area (Table 4), with a consequent decrease in the availability of water for drinking, agricultural and industrial purposes [59]. Indeed the Cannara well field is characterised by a reservoir with a withdrawable flow rate greater than 30 l/s not currently substitutable with other supply sources, also considering the impact of climate change on the groundwater resources. The subsidence is localized in a topographically depressed sector of the valley that was occupied up to the V-VI century by a large lake and marshy area called “Lacus Umber” [34] (Figure 2c). The maximum thickness of the recent alluvial sediments is estimated in this area of about 150 m [49] Famiani indicates a relatively high regional subsidence rate of the hanging-wall block and suggests that the basin-bounding faults are capable to counteract the regional uplift [46] Pucci. In addition, significant historical and instrumental seismicity suggests that these faults are still active and responsible for the area's seismic activity. Further study is needed in the whole VU to observe the ground response to groundwater level variations and to understand if the compaction of the deep aquifer will cause a decrease in available water resources. At the same time, this methodological approach and the availability of large datasets of MInSAR products could provide prompts for the relation between the bedrock organisation with the likely presence of faulted bedrock and the deforming valley deposits filling the extensional basins. The analysis of more recent data will confirm the decrease in the subsidence phenomenon and, added to the data here presented can help the description of the tectonic activity present in the valley.

Author Contributions: C.A.B.and F.M. have equally contributed to the paper

Data Availability Statement: The ERS, ENVISAT and SCOSMO Sky-Med PS time series are produced and can be required within PST-A “Extraordinary Plan for Environmental Remote Sensing”), funded by the former Italian Ministry of Environment, Land and Sea (MATTM) - http://www.pcn.minambiente.it/).

Acknowledgements: In this section, you can acknowledge any support given which is not covered by the author contribution or funding sections. This may include administrative and technical support, or donations in kind (e.g., materials used for experiments).

Conflicts of Interest: The authors declare no conflict of interest.

References

1. Guo H., Wang L., Chen F., Liang D. (2014). Scientific big data and Digital Earth. Chin. Sci. Bull. (2014) 59(35):5066–5073. Doi 10.1007/s11434-014-0645-3
2. Guo H. (2017) Big Earth data: A new frontier in Earth and information sciences, Big Earth Data, 1:1-2, 4-20. Doi: 10.1080/20964471.2017.1403062
3. Casu F., Manunta M., Agramb P.S., Crippen R.E. Big Remotely Sensed Data: tools, applications and experiences (2017), Remote Sensing of Environment 202 (2017) 1–2. Doi: 10.1016/j.rse.2017.09.013
4. Gurusamy V., Kannan S., Nandhini K. (2017). The Real-Time Big Data Processing Framework: Advantages and Limitations. Vol. 5, Issue-12 E-ISSN: 2347-2693, IJCSE Doi: 10.26438/ijcse/v5i12.305312
5. De Luca C., Zinno I., Manunta M., Lanari R., Casu F., Large areas surface deformation analysis through a cloud computing P-SBAS approach for massive processing of DInSAR time series, Remote Sensing of Environment, Vol. 202, 2017, pp. 3-17, https://Doi.org/10.1016/j.rse.2017.05.022.
6. Cigna F., Tapete D. (2021) Sentinel-1 Big Data Processing with P-SBAS InSAR in the Geohazards Exploitation Platform: An Experiment on Coastal Land Subsidence and Landslides in Italy. Remote Sens. 2021, 13, 885. https:// Doi.org/10.3390/rs13050885
7. Costantini, M., Ferretti A., Minati F., Falco S., Trillo F., Colombo D., Novali F., Malvarosa F., Mammone C., Vecchioli F., Rucci A., Fumagalli A., Allievi J., Ciminelli M. ., Costabile S., 2017. Analysis of surface deformations over the whole Italian territory by interferometric processing of ERS, ENVISAT and COSMO-SkyMed radar data. Remote Sens. Environ. http://dx.Doi.org/10.1016/j.rse.2017.07.017.
8. Solari L, Del Soldato M, Bianchini S, Ciampalini A, Ezquerro P, Montalti R, Raspini F and Moretti S (2018) From ERS 1/2 to Sentinel-1: Subsidence Monitoring in Italy in the Last Two Decades. Front. Earth Sci. 6:149. Doi: 10.3389/feart.2018.00149
9. Terzaghi, K.V. Relation between soil mechanics and foundation engineering. In Proceedings of the 1936 International Conference on Soil Mechanics and Foundation Engineering, Boston, MA, USA, 22–26 June 1936.
10. Cigna F., Jordan H., Bateson L, McCormack H., Roberts C. (2015) Natural and Anthropogenic Geohazards in Greater London Observed from Geological and ERS-1/2 and ENVISAT Persistent Scatterers Ground Motion Data: Results from the EC FP7-SPACE PanGeo Project. Pure Appl. Geophys. 172, 2965–2995 (2015). https://Doi.org/10.1007/s00024-014-0927-3
11. Dong S., Samsonov S., Yin H., Ye S., Cao Y. (2014) Time-series analysis of subsidence associated with rapid urbanisation in Shanghai, China measured with SBAS InSAR method. Environ Earth Sci 72, 677–691 (2014). https://Doi.org/10.1007/s12665-013-2990-y
12. Chaussard, E., Wdowinski, S., Cabral-Cano, E.,, Amelung, F. C. (2014). Land subsidence in central Mexico detected by ALOS InSAR time series. Remote Sensing of Environment, 140, 94-106. https://Doi.org/10.1016/j.rse.2013.08.038
13. Murgia, F.; Bignami, C.; Brunori, C.A.; Tolomei, C.; Pizzimenti (2019), L. Ground deformations controlled by hidden faults: Multifrequency and multitemporal InSAR techniques for urban hazard monitoring. Remote Sens. 2019, 11, 2246. Doi:10.3390/rs11192246
14. Cigna, F., & Tapete, D. (2022). Land subsidence and aquifer-system storage loss in Central Mexico: A quasi-continental investigation with Sentinel-1 InSAR. Geophysical Research Letters, 4, e2022GL098923. https://Doi.org/10.1029/2022GL098923
15. Delgado Blasco, J.M.; Foumelis, M.; Stewart, C.; Hooper, A. Measuring Urban Subsidence in the Rome Metropolitan Area (Italy) with Sentinel-1 SNAP-StaMPS Persistent Scatterer Interferometry. Remote Sens. 2019, 11, 129. Doi: 10.3390/rs11020129
16. Stramondo, S.; Saroli, M.; Tolomei, C.; Moro, M.; Doumaz, F.; Pesci, A.; Boschi, E. Surface movements in Bologna (Po Plain-Italy) detected by multitemporal DInSAR. Remote Sens. Environ. 2007, 110, 304–316
17. Antonellini M., Giambastiani B.M.S., Greggio N., Bonzi L., Calabrese L., Luciani P., Perini L., Severi P. (2019). Processes governing natural land subsidence in the shallow coastal aquifer of the Ravenna coast, Italy. Catena, 172, 76-86. Doi: 10.1016/j.catena.2018.08.019
18. Polcari M, lbano M, Montuori A, Bignami C, Tolomei C, Pezzo G, Falcone S, La Piana C, Doumaz F, Salvi S, Stramondo S. (2018) InSAR Monitoring of Italian Coastline Revealing Natural and Anthropogenic

Ground Deformation Phenomena and Future Perspectives. Sustainability. 2018; 10(9):3152. https://Doi.org/10.3390/su10093152

19. Fiaschi S., Fabris M., Floris M, Achilli V. (2018) Estimation of land subsidence in deltaic areas through differential SAR interferometry: the Po River Delta case study (Northeast Italy), International Journal of Remote Sensing, 39:23, 8724-8745. Doi: 10.1080/01431161.2018.1490977
20. Teatini, P., Tosi L., Strozzi T., Carbognin L., Cecconi G., Rosselli R., Libardo S. (2010) Resolving land subsidence within the Venice Lagoon by persistent scatterer SAR interferometry. J. Phys. Chem. Earth. Doi:10.1016/j.pce.2010.01.002
21. Solari, L.; Ciampalini, A.; Raspini, F.; Bianchini, S.; Moretti, S. PSInSAR analysis in the pisa urban area (Italy): A case study of subsidence related to stratigraphical factors and urbanization. Remote Sens. 2016, 8, 120. https://Doi.org/10.3390/rs8020120
22. Raspini F., Cigna F., Moretti S. (2012) Multi-temporal mapping of land subsidence at basin scale exploiting Persistent Scatterer Interferometry: case study of Gioia Tauro plain (Italy), Journal of Maps, 8:4, 514-524. Doi: 10.1080/17445647.2012.743440
23. Cianflone, G., Tolomei, C., Brunori, C. A., Dominici, R. (2016). InSAR time series analysis of natural and anthropogenic coastal plain subsidence: the case of Sibari (Southern Italy). Remote Sens. 7, 16004–16023. Doi: 10.3390/rs71215812
24. Brunori C.A., Bignami C. Albano M., Zucca F. Samsonov S., Groppelli G. Norini G. Saroli M., Stramondo S. (2015), Land subsidence, Ground Fissures and Buried Faults: InSAR Monitoring of Ciudad Guzmán (Jalisco, Mexico). Remote Sens. 2015, 7, 8610-8630. Doi:10.3390/rs70708610
25. Navarro-Hernández, M. I., Tomás, R., Lopez-Sanchez, J. M., Cárdenas-Tristán, A., & Mallorquí, J. J. (2020). Spatial analysis of land subsidence in the San Luis Potosí valley induced by aquifer overexploitation using the coherent pixels technique (CPT) and sentinel-1 insar observation. Remote Sensing, 12(22), 3822. Doi:10.3390/rs12223822
26. Gourmelen N., Amelung F., Casu F., Manzo M., Lanari R. . (2007) Mining-related ground deformation in Crescent Valley, Nevada: implications for sparse GPS networks Geophys. Res. Lett., 34 (9) (2007), Article L09309. Doi: 10.1029/2007GL029427
27. Cianflone G., Tolomei C., Brunori C.A., Monna S., Dominici R. (2018) Landslides and Subsidence Assessment in the Crati Valley (Southern Italy) Using InSAR Data. Geosciences 2018, 8 (2), 67. https://Doi.org/10.3390/geosciences8020067.
28. Hu L., Dai K., Xing C., Li Z., Tomás R., Clark B., Shi X., Chen M., Zhang R., Qiu Q., Lu Y. (2019) Land subsidence in Beijing and its relationship with geological faults revealed by Sentinel-1 InSAR observations. International Journal of Applied Earth Observation and Geoinformation. 82. 10.1016/j.jag.2019.05.019.
29. Guzzetti F., Manunta M., Ardizzone F., Pepe A., Cardinali M., Zeni G., Reickenbach P., Lanari R. (2009), Analysis of ground deformation detected using the SBAS-DInSAR technique in Umbria, Central Italy. Pure Appl. geophys. 166 (2009) 1425–1459, 0033–4553/09/081425–35. Doi: 10.1007/s00024-009-0491-4.
30. Scarsella F. (1951) - Un raggruppamento di pieghe dell'Appennino umbro-marchigiano. La catena M. Nerone-M. Catria-M. Cucco-M. Penna-Colfiorito-M. Serano. Bollettino del Servizio Geologico d'Italia, 73, 309-20.
31. Lavecchia, G., Barchi, M., Brozzetti, F., & Menichetti, M. (1994). Sismicità e tettonica nell'area umbro-marchigiana. Boll. Soc. Geol. It, 113, 483-500.
32. Barchi M.R., Lemmi M. (2015). NOTE ILLUSTRATIVE della CARTA GEOLOGICA D'ITALIA alla scala 1:50.000, Foglio 324 Foligno. ISPRA-Servizio Geologico d'Italia https://www.isprambiente.gov.it/Media/carg/note_illustrative/324_Foligno.pdf
33. Tarquini S., I. Isola, M. Favalli, A. Battistini, G. Dotta (2023). TINITALY, a digital elevation model of Italy with a 10 meters cell size (Version 1.1). Istituto Nazionale di Geofisica e Vulcanologia (INGV). https://Doi.org/10.13127/tinitaly/1.1
34. Camerieri P., Manconi D. (2008), "Le centuriazioni della Valle Umbra da Spoleto a Perugia", in XVII International Congress of Classical Archaeology, Roma 22-26 Sept. Poster Session: Landscape Archaeology / Archeologia del Paesaggio, Bollettino di Archeologia on line.
35. Conti M. A. & Girotti O. (1977) - Il Villafranchiano nel «lago tiberino », ramo sud-occidentale: schema stratigrafico e tettonico. Geol. Romana, 16, 67-80, 13 fl., 1 tab.

36. Ambrosetti P., Carboni M.G., Conti M.A., Esu D., Girotti O., La Monica G.B., Landini B., Parisi G. (1987) - Il Pliocene ed il Pleistocene inferiore del bacino del Fiume Tevere nell'Umbria meridionale. Geogr. Fis. Dinam. Quat., 10, 10-33.
37. Basilici G. (1997) - Sedimentary facies in an extensional and deep-lacustrine depositional system: the Pliocene Tiberino Basin, Central Italy. Sedimentary Geology, 109(1-2), 73-94. https://Doi.org/10.1016/S0037-0738(96)00056-5
38. Coltorti M., Pieruccini P., 1997. Middle-Upper Pliocene 'compression' and Middle Pleistocene 'extention' in the modelling of the East Tiber Basin (Central Italy): from 'perched' to 'extentional basin in the Northern Apennines. Il Quaternario 10(2) 521-528.
39. Bucci, F., Mirabella, F., Santangelo, M., Cardinali, M., Guzzetti, F. (2016). Photogeology of the Montefalco Quaternary basin, Umbria, Central Italy. Journal of Maps, ISSN: 1744-5647. Doi: 10.1080/17445647.2016.1210042.
40. Ge.Mi.Na. (1962). Ligniti e torbe dell'Italia continentale. Geomineraria nazionale, 1–319 (Italian).
41. Cardinali, M., Antonini, G., Reichenbach, P., Guzzetti, F. (2001), Photo-geological and landslide inventory map for the Upper Tevere River basin. CNR, Gruppo Nazionale per la Difesa dalle Catastrofi Idrogeologiche, Publication n. 2154, scale 1:100,000. http://geomorphology.irpi.cnr.it/publications/repository/public/maps/UTR-data.jpg/view
42. Martinetto, E., Bertini, A., Basilici, G., Baldanza, A., Bizzarri, R., Cherin, M., Gentili, S., & Pontini, M. R. (2014). THE PLANT RECORD OF THE DUNAROBBA AND PIETRAFITTA SITES IN THE PLIO-PLEISTOCENE PALAEOENVIRONMENTAL CONTEXT OF CENTRAL ITALY . Alpine and Mediterranean Quaternary, 27(1), 29–72. Retrieved from https://amq.aiqua.it/index.php/amq/article/view/70
43. Mutti E.,Ricci Lucchi F. (1978). Turbidites of the northern Apennines: introduction to facies analysis, International Geology Review, 20:2, 125-166, Doi: 10.1080/00206817809471524
44. Centamore E., Deiana G., Micarelli A., Potetti M. (1986) - Il Trias-Paleogene delle Marche. Studi Geologici Camerti, Vol. Spec. "La geologia delle Marche": 9-27.
45. Cresta S., Monechi S., Parisi G., Baldanza A., Reale V. (1989) - Stratigrafia del Mesozoico e Cenozoico nell'area umbro-marchigiana. Itinerari geologici sull'Appennino Umbro-marchigiano. Mem. Descr. della Carta Geol. d'It., 39.
46. Barchi, M. (2010). The Neogene-quaternary evolution of the Northern ApeREFines: Crustal structure, style of deformation and seismicity. In M. Beltrando, A. Peccerillo, M. Matte, S. Conticelli, & C. Doglioni (Eds.), The geology of Italy, Journal of the Virtual Explorer, Electronic Edition, 36, paper 10.
47. Pucci, S., Mirabella, F., Pazzaglia, F., Barchi, M. R., Melelli, L., Tuccimei, P., et al. (2014). Interaction between regional and local tectonic forcing along a complex Quaternary extensional basin: Upper Tiber Valley, Northern Apennines, Italy. Quaternary Science Reviews, 102, 111–132. https://Doi.org/10.1016/j.quascirev.2014.08.009
48. Malinverno, A. and Ryan, W.B.F. (1986) Extension in the Tyrrhenian Sea and Shortening in the Apennines as Result of Arc Migration Driven by Sinking of the Lithosphere. Tectonics, 5, 227-245. http://dx.Doi.org/10.1029/TC005i002p00227
49. Martini, I.P. and Sagri, M. (1993) Tectono-Sedimentary Characteristics of Late Miocene Quaternary Extensional Basins of the Northern Apennines, Italy. Earth-Science Reviews, 34, 197-133. https://Doi.org/10.1016/0012-8252(93)90034-5
50. Famiani D., Brunori C.A., Pizzimenti L., Cara F., Caciagli M., Melelli L., Mirabella F., Barchi M. R. (2020). Geophysical reconstruction of buried geological features and site effects estimation of the Middle Valle Umbra basin (central Italy). Engineering Geology, 105543. https://Doi.org/10.1016/j.enggeo.2020.105543
51. Rovida A., Locati M., Camassi R., Lolli B., Gasperini P., Antonucci A. (eds), 2021. Italian Parametric Earthquake Catalogue (CPTI15), version 3.0. Istituto Nazionale di Geofisica e Vulcanologia (INGV). https://Doi.org/10.13127/CPTI/CPTI15.3
52. Vetturini E. (1995). Terre e acque in valle Umbra, Bastia, 1995, pag. 74)
53. Ferretti A., Fumagalli A., Novali F., Prati C., Rocca F, Rucci O. (2011), A new algorithm for processing interferometric data-stacks: SqueeSAR IEEE Transactions on Geoscience and Remote Sensing 49 (9), 3460-3470. Doi: 10.1109/TGRS.2011.2124465.

54. Costantini M., Falco S., Malvarosa F., Minati F., Trillo F., Vecchioli F. (2014). Persistent Scatterer Pair Interferometry: Approach and Application to COSMO-SkyMed SAR Data. IEEE Journal of Selected Topics In Applied Earth Observations And Remote Sensing, vol. 7, no. 7. Doi: 10.1109/JSTARS.2014.2343915
55. Costantini M., Falco S., Malvarosa F., Minati F., Trillo F. (2009). Method of persistent scatterer pairs (PSP) and high resolution SAR interferometry. 2009 IEEE International Geoscience and Remote Sensing Symposium, Cape Town, South Africa, 2009, pp. III-904-III-907. Doi: 10.1109/IGARSS.2009.5417918.
56. Dalla Via G., Crosetto M., Crippa B. (2012), Resolving vertical and east-west horizontal motion from differential interferometric synthetic aperture radar: The L'Aquila earthquake: resolving z and e-w motion from D-InSAR. J. Geophys.: Solid Earth, vol 117, 2012. Doi: 10.1029/2011JB008689
57. Fuhrmann T., Garthwaite M.C. (2019). Resolving three-dimensional surface motion with InSAR: Constraints from multi-geometry data fusion. Remote Sens. 2019, 11, 241. Doi: 10.3390/rs11030241
58. Pepe, A.; Solaro, G.; Calò, F.; Dema, C. A Minimum Acceleration Approach for the Retrieval of Multiplatform InSAR Deformation Time Series. IEEE J. Sel. Top. Appl. Earth Obs. Remote Sens. 2016, 9, 3883–3898. Doi: 10.1109/JSTARS.2016.2577878
59. Beretta, G. P., Avanzini, M., Marangoni, T., Burini, M., Schirò, G., Terrenghi, J., & Vacca, G. (2018). Groundwater modelling of the withdrawal sustainability of Cannara artesian aquifer (Umbria-Italy). ACQUE SOTTERRANEE, 7(3), 47-60. Doi: 10.7343/as-2018-333